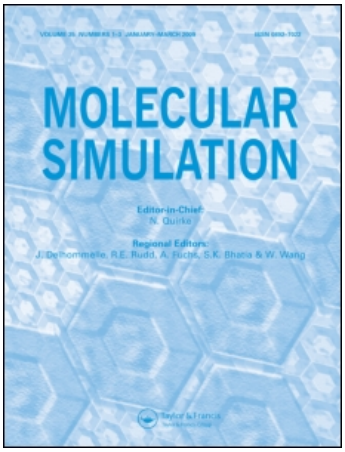

Molecular Simulation
Publication details, including instructions for authors and subscription information:
http://www.informaworld.com/smpp/title~content=t713644482

Molecular Dynamics Simulations of the Goethite-water Interface

Robert M. Shroll[a]; T. P. Straatsma[a]
[a] Computational Biochemistry, Biophysics and Biology Group, Theory, Modeling and Simulation Environmental Molecular Sciences Laboratory, Pacific Northwest National Laboratory, Richland, WA 99352, USA

Online publication date: 26 October 2010

To cite this Article Shroll, Robert M. and Straatsma, T. P.(2003) 'Molecular Dynamics Simulations of the Goethite-water Interface', Molecular Simulation, 29: 1, 1 — 11
To link to this Article: DOI: 10.1080/0892702031000065683
URL: http://dx.doi.org/10.1080/0892702031000065683

Molecular Simulation, 2003 Vol. 29 (1), pp. 1–11

Molecular Dynamics Simulations of the Goethite–Water Interface

ROBERT M. SHROLL and T.P. STRAATSMA*

Computational Biochemistry, Biophysics and Biology Group, Theory, Modeling and Simulation Environmental Molecular Sciences Laboratory, Pacific Northwest National Laboratory, Richland, WA 99352, USA

(Received May 2002, In final form May 2002)

Classical molecular models of the goethite mineral are presented for both a periodically replicated bulk slab and for a finite fragment. Potential energy functions for the mineral models were developed within the AMBER force field [Cornell, W.D., Cieplak, P., Bayly, C.I., Gould, I.R., Merz, K.M., Ferguson, D.M., Spellmeyer, D.C., Fox, T., Caldwell, J.W. and Kollman, P.A. "A second generation force field for the simulation of proteins, nucleic acids and organic molecules," *J. Am. Chem. Soc.* 117 (1995) 5179–5197], which facilitates biogeochemical applications. Intramolecular potential parameters were chosen to yield a mineral structure with flexible surface hydroxyl groups. The electrostatic potential for a goethite slab was determined from a periodic Unrestricted Hartree–Fock calculation and used to assign point charges to the mineral atoms. The models were solvated in water and their effect on solution structure is shown to be very similar, predicting oscillations in solvent density near the mineral surface and structured orientation of water molecules.

Keywords: Molecular dynamics simulation; Goethite–water interface; Water molecules; Hartree–Fock calculation

INTRODUCTION

Mineral surfaces affect the mobility of contaminants in soils through sorption processes. They also provide the scaffolding for biofilms and aid in anaerobic bacterial respiration by providing electron acceptors. Ferric oxides and oxyhydroxides are important contributors to adsorption processes in the soil subsurface for a large number of cations and anions. This is due in part to their frequent occurrence as minerals and amorphous coatings with high specific area [1]. Goethite crystals have specific areas in the range of 50–200 m^2/g and possess strong affinity for heavy metal contaminants [1–3]. The predominant crystal plane of goethite needles has been shown to be (110) along the *c* direction and (021) at the needles' end [1,4].

Here we present parameterized classical simulation models for the goethite mineral. They are intended to provide molecular level insight into goethite interactions in the soil subsurface and were developed using a potential consistent with the AMBER force field [5]. This choice of potential was made to facilitate their future introduction into the simulations of Lins and Straatsma [6], in order to describe interactions between a bacterial membrane and a mineral surface. Using the AMBER potential enables the models to be easily adapted to biogeochemical simulations such as those of Teppen *et al.* [7] and Yu *et al.* [8].

The AMBER force field cannot address problems associated with acid-base reactions at the mineral surface, because it does not allow for bond dissociation. Progress has been made toward our understanding of select mineral–water interfaces using experimental techniques such as high-resolution X-ray reflectivity [9–11]. Unfortunately, these methods do not provide the complete atomic level structure. However, theoretical [3,12] and empirical [13] methods have provided a reasonable description of the protonation states of the surface functional groups, which are constant in our simulations. Our particular approach ensures consistency between the mineralogical force field and the AMBER force field commonly used in biochemical research [14,15]. In addition, consistency with AMBER allows the use of the extended simple point charge (SPC/E) water

*Corresponding author.

ISSN 0892-7022 print/ISSN 1029-0435 online
DOI: 10.1080/0892702031000065683

model for investigation of surface solvation. The SPC/E potential has been extensively tested in a variety of contexts associated with ion and surface solvation, and moreover, is known to give good dielectric behavior [16–19]. The SPC/E model is also less demanding computationally than, for example, the polarizable/dissociable model employed by Rustad *et al.* [3] and can be used in much larger systems for longer times.

Our goethite models have been parameterized for use as either a 2D periodically replicated mineral slab or as a finite mineral fragment. Simulations using slabs are able to predict surface properties without the influence of edges, which often makes them preferable to simulations employing small mineral fragments. However, there are several situations where a fragment model has distinct advantages over the corresponding slab model. For computer simulations in constant pressure ensembles (i.e. NPT or μPT) the pressure is held constant and the volume of the simulation is allowed to fluctuate. These volume fluctuations are defined by corresponding fluctuations in the length of the simulation cell sides. When simulating crystalline mineral slabs, the mineral's rigid nature hinders these fluctuations. For instance, a slab periodically replicated in the *xy*-plane would restrain the dimensions of the plane and pressure equilibration would rely on fluctuations in the *z*-cell length. For many applications such as modeling clay minerals, this is of no concern. However, there are other cases where this restraint is a significant perturbation and unwanted. An example of such a situation is when a rigid slab model is used in a NPT simulation with a slab model for a liquid crystal. The mineral places an undesirable restraint on the motion of the liquid crystal and modifies the properties of the system. This situation is remedied by using a mineral fragment, since the volume fluctuations are not restricted.

The crucial part of the mineral model development, as with any classical molecular model, is the development of an accurate potential. The potential energy parameters were determined for a small mineral fragment and for a periodic slab. The small mineral fragment was designed to reproduce the potential interactions of the mineral surface while minimizing the influence of the edges. This was done by fitting the mineral fragment point charges to the mineral slab electrostatic potential (ESP), which was obtained from a periodic Hartree–Fock calculation. The values of the ESP fit charges fall within the same range as those based on Mulliken charges and on small cluster restricted high-spin open-shell Hartree–Fock (ROHF) calculations. However, mineral fragment point charges derived in this manner reproduced the bulk slab ESP much better than the Mulliken charges. Parameters for the slab potential were taken from the center region of the fragment. The slab model was then used to test for the influence of the edges on the properties of the fragment model.

A comparison of the radial distribution functions for water molecules with the (110) mineral surface of the two models reveals that the structuring of the solvent near the mineral surface is very similar. This indicates that the fragment model is appropriate to study the solution structure near the (110) mineral surface. The distribution functions show distinctive structuring of the solution near the mineral surface. A few water molecules interact strongly with the mineral surface, forming into ordered rows across the surface. And a layer of increased solvent density develops 2 Å from the first solvent accessible plane of the mineral surface. The orientation of water molecules associated with these two features is not isotropic and results in each possessing a net dipole moment.

MINERAL MODEL

The intramolecular potential parameters used in Eq. (A1) (see Appendix A) for the mineral models were $K_r = 5.0 \times 10^5\,\mathrm{kJ/(mol\,nm^2)}$ for Fe–O bonds, $K_\theta = 5.0 \times 10^3\,\mathrm{kJ/(mol\,radian^2)}$ for Fe–O–Fe and O–Fe–O angles, and $V_{n=4}/2 = 4.184\,\mathrm{kJ/mol}$ for O–Fe–O–H dihedral angles. The intermolecular Lennard–Jones parameters for hydroxyl groups were taken from the AMBER force field and parameters for iron were adapted from Giammona [20]. The values of the equilibrium positions r_{eq} and θ_{eq} for the (110) plane were taken directly from the structure of Rustad *et al.* [3,21] and have been omitted due to their large number. The mineral structure at the equilibrium positions is shown in Fig. 1. Stiff force constants were chosen in order to simulate a rigid structure. Bonds and angles formed with hydrogen were fixed using SHAKE [22]. The value for V_n was chosen to be in agreement with other torsional potentials for hydroxyl groups in the AMBER force field. This allowed the surface hydroxyl groups to rotate during the course of the simulation. All values of V_n for torsions other than surface hydroxyl groups were set to zero, since these motions are restrained due to the rigid nature of the crystalline structure.

The atom-centered point charges q_i of Eq. (A1) were determined using the RESP method [23] as implemented in NWChem [24]. The charges were fit to the ESP of a 2D goethite slab based on a periodic Unrestricted Hartree–Fock (UHF) calculation using CRYSTAL98 [25,26]. These calculations were performed on the slab in order to accurately parameterize the electrostatic potential of the bulk mineral [27]. Coordinates for the slab unit cell were taken from Rustad *et al.* [3,21], with a unit cell consisting of

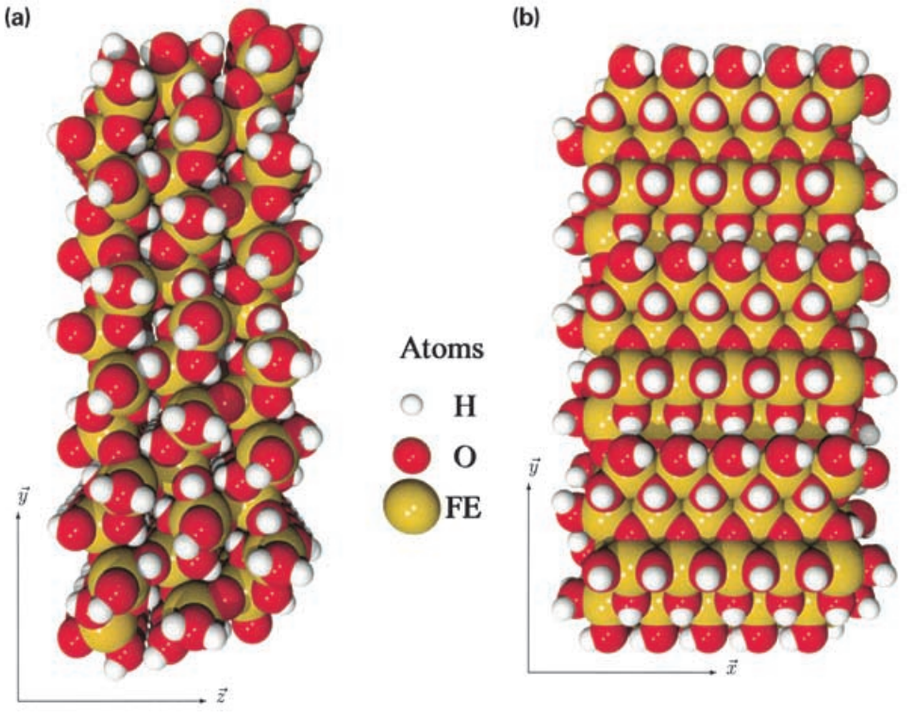

FIGURE 1 The goethite mineral fragment and dipole orientation axes. Iron atoms are rendered in gold, oxygen atoms in red, and hydrogen atoms in white: (a) the (110) goethite surface; (b) the edge of the goethite fragment model. (Colour version available online)

54 atoms. This corresponds to three goethite bulk unit cells with 16 atoms each and two dissociated water molecules used to terminate the (110) surface. The slab is therefore three bulk unit cells thick in the direction of the z-axis and replicated in the x- and y-axes. A 6-31G* basis set was used [28–30] after two modifications. The most diffuse iron *sp*-function was excluded to avoid possible linear dependencies and the iron *f*-function was excluded, since CRYSTAL98 does not allow for functions of higher angular momentum than *d*. The high-spin antiferromagnetic solution was obtained.

The UHF wavefunction was used to produce a set of ESP values, which were fit by atom-centered point charges of a mineral fragment. Values of the ESP were determined over a regular grid of points ranging from no closer than 2 Å from surface atoms to 5 Å. Point charges were fit to a total 4204 grid points by the RESP method. Varying ranges and densities of ESP points were tested and showed little effect on the resulting charges over a wide range.

The mineral fragment consisted of 978 atoms and is shown in Fig. 1. The (110) surface corresponds to 15 slab unit cells in a 5×3 arrangement as displayed in Fig. 2a. The edge of the fragment is shown in Fig. 2b. It has a 1×3 arrangement of slab cells, where each of these is composed of three bulk unit cells. The edge sites created by using a small subsection of the infinite slab were terminated by 56 water molecules. Two methods of terminating the edges were compared, one with no dissociation of water molecules and one with partial dissociation. Both methods produced similar point charges and reproduced the ESP above the (110) surface well. The edge sites of the final model were terminated with partially dissociated water molecules, because the edge termination did not noticeably affect the properties of the (110) surface. Some water molecules were bonded to iron atoms through their oxygen atoms and some were dissociated. Dissociated water molecule hydroxyl groups were bonded to iron atoms on the mineral surface and a hydrogen atom was bonded to the neighboring mineral oxygen atom. The edge sites were terminated prior to the RESP fitting procedure.

The RESP fitting procedure was done with the addition of several constraints. All of the 15 bulk slab cells were constrained to have zero net charge. For each slab cell, symmetrically equivalent atoms were constrained to have equal charges. As shown in Fig. 2a, the cells were also divided into five cell types that were constrained to have equivalent point charges. Water molecules used to terminate the edges, not the (110) face, were constrained to have equal point charges. The variability of the Mulliken oxygen charges was much greater than those of the iron or hydrogen charges. In the RESP fitting all iron atoms were constrained to have $1.6e$ charge and all hydrogen atoms were constrained to have $0.5e$ charge. These values fall within the range of charges

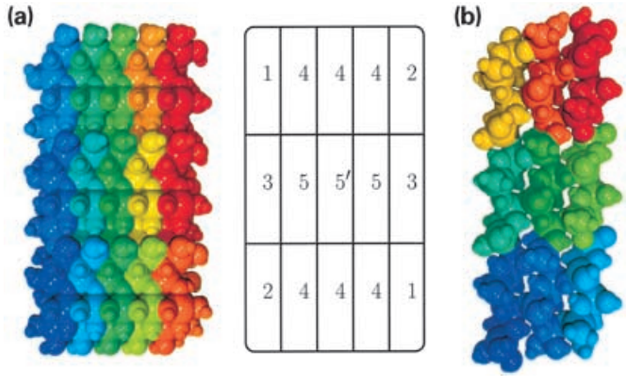

FIGURE 2 Color coded representations of the goethite fragment simulation cells. (a) The (110) mineral surface consisting of a 5×3 surface of slab unit cells with varying edge terminations depending on location. Each mineral cell is designated by a number in the right diagram. Cells with equivalent numbers were constrained in the RESP fitting procedure to have equivalent point charge. The cell labeled 5′ was used for the mineral slab model. (b) The mineral fragment model viewed from the side. Each slab unit cell is composed of three bulk unit cells with terminating atoms. (Colour version available online)

based on ROHF calculations of a cluster as shown in Fig. 3. The point charges of a mineral fragment were derived from the ESP of a 2D-slab. This causes the edge sites to be located relatively far from the ESP grid points and fixing the iron and hydrogen charges helped assure the integrity of resulting ESP. This leaves the charges on the oxygen atoms as the fitting parameters. The resulting distribution of charges for the oxygen atoms is shown in Figs. 4 and 5.

Cluster calculations could have been used to determine the charges of the atoms alone. However, unambiguous assignment of atom charges requires the use of large clusters. Also, the local electronic structure of surfaces can be different from that of bulk and conclusions drawn from cluster calculations may be misleading [31]. The use of Mulliken charges exclusively is prone to variable ESP signatures based on basis set size. For this system, the calculated Mulliken charges do an inadequate job of quantitatively reproducing the ESP of the mineral surface. However, by fitting the oxygen charges using the RESP method the proper ESP is obtained as shown in Fig. 6.

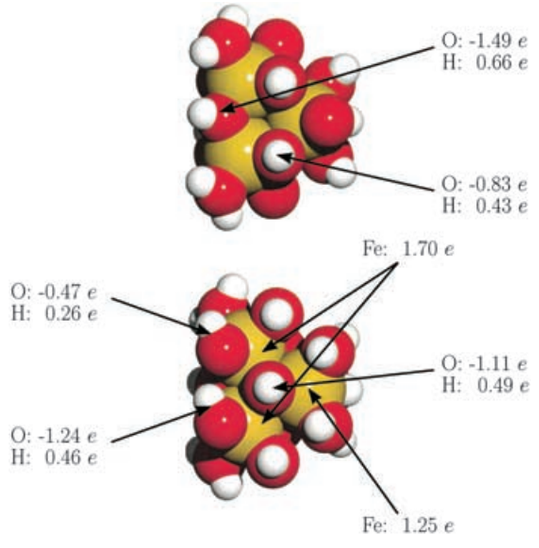

FIGURE 3 A small cluster based on the Rustad *et al.* [3] structure for goethite. The charges were obtained by the RESP method and are shown for some atoms. The ROHF method was used with a 6-31G* basis set. (Colour version available online)

COMPUTATIONAL METHODS

Classical molecular dynamics simulations of the mineral–water system were performed using the high-performance parallel computational chemistry package NWChem [24]. All equilibrium averaging was performed in the NPT ensemble using periodic boundary conditions. A target temperature of 300 K was maintained using Berendsen's thermostat with a temperature relaxation time of 0.1 ps [32]. The target pressure of 1.025×10^5 Pa was maintained using Berendsen's piston with a pressure relaxation time of 0.5 ps and a system compressibility of 4.53×10^{-10} m^2N^{-1} with anisotropic coordinate scaling. The leapfrog integration method was used with a 2 fs time step [33]. A shorter time step was not needed, because constraints removed vibrations involving hydrogen. A 1.0 nm cutoff was used for long and short-range interactions. The Coulomb part of the potential energy was evaluated for the periodically replicated system using the smooth particle-mesh Ewald method with 32 grid points per dimension [34]. The SPC/E water model was used [35]. Each SPC/E water molecule consists of three atomic sites and has a rigid geometry with bond lengths of 1 Å and a tetrahedral bond angle of 109.47°.

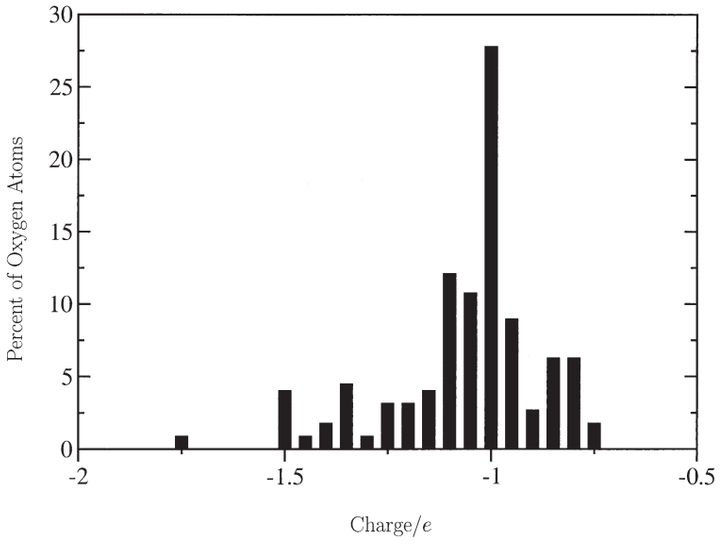

FIGURE 4 The distribution of oxygen charges for the goethite fragment. Charges for the oxygen atoms were determined from the RESP fit to the bulk slab electrostatic potential.

Mineral Fragment

The mineral fragment shown in Fig. 1 was placed in a 5.52 nm × 6.85 nm × 5.00 nm box of 5869 water molecules. The system was allowed to equilibrate for 1 ns in the NPT ensemble. After equilibration the new box dimensions were 3.44 nm × 4.74 nm × 3.91 nm. This system was re-solvated in a 7.00 nm × 7.00 nm × 7.00 nm box with 10831 water molecules and a 1.2 ns trajectory was obtained of the resulting mineral water system. The box dimension had equal sides, which fluctuated about 6.94 nm in length. Property averaging was done after the first 200 ps.

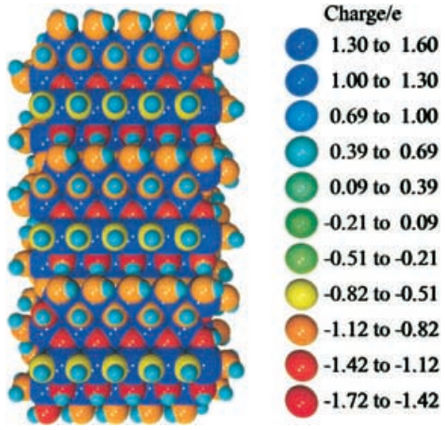

FIGURE 5 The distribution of atomic charges for the goethite fragment. Iron atoms have a charge of 1.6*e* and hydrogen atoms have a charge of 0.5*e*. Charges for the oxygen atoms were determined from the RESP fit to the bulk slab electrostatic potential. (Colour version available online)

Mineral Slab

The mineral slab model was developed from the mineral fragment. Force field parameters were taken from the 5′ slab unit cell in the center of the fragment shown in Fig. 2a. This cell was chosen since of all the cells, the central cell is in an environment most closely resembling a slab. A 2.40 nm × 2.20 nm surface of 864 atoms was formed from 16 slab unit cells. The average distance between the centers of the mineral layers in the NPT ensemble was 14.26 nm and the volume between the mineral layers was filled with 2301 water molecules. This was used as the starting configuration for a 1 ns molecular dynamics simulation in the NPT ensemble. Property averaging was done after the first 100 ps.

RESULTS AND DISCUSSION

The periodic UHF ESP for the (110) goethite slab predicts distinctive alternating positive and negative regions as shown by the left image in Fig. 6. Capturing this feature is an essential element in accurately parameterizing the classical simulations of the goethite mineral, because electrostatic interactions play a significant role in the system's behavior. The bulk slab ESP was used in the RESP fitting procedure for the mineral fragment point charges. The resulting point charges produce an ESP above the mineral fragment (110) surface that closely resembles that of the bulk material as shown in the comparison made in Fig. 6. This design is intended for future introduction into bacterial membrane simulations where a periodically replicated mineral surface would have undesirable consequences.

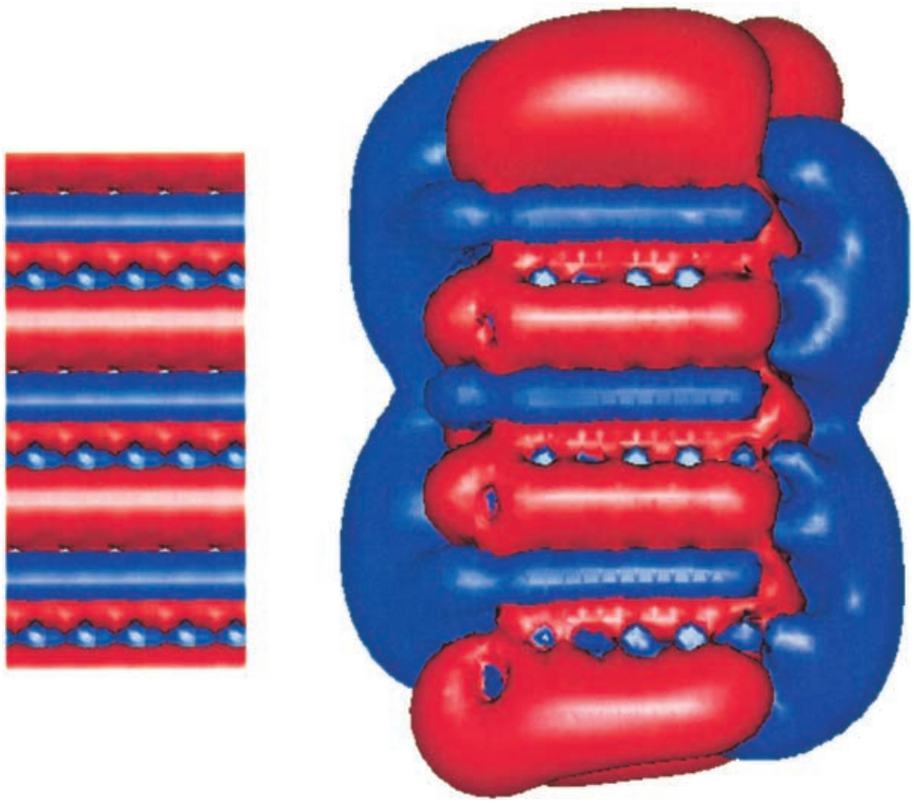

FIGURE 6 The goethite fragment electrostatic potential. The figure on the left is the electrostatic potential calculated from the periodic Unrestricted Hartree–Fock wave-function. It may be replicated in the *xy*-plane (plane of the figure) to reproduce the ESP of the mineral slab. The dimensions shown here are 5 unit cells in width and 3 unit cells in height, which corresponds to the surface dimensions of the fragment. The figure on the right is for the mineral fragment and is calculated from the set of RESP point charges. For both figures, the $-25\,e$·kJ/mol isosurface is red and the $25\,e$·kJ/mol isosurface is blue. (Colour version available online)

The average structure of the mineral–water interface is shown by radial distribution functions in Fig. 7. Distribution functions are presented for both the slab and the fragment models. These functions were derived from water molecules located directly above the (110) surfaces of the minerals. Water molecules were sampled from a set of cylinders (15 per side for the fragment and 12 per side for the slab) centered on surface atoms with 4.0 Å radii. The cylinders were made large enough to overlap, however, water molecules were only counted once. Plots were normalized using

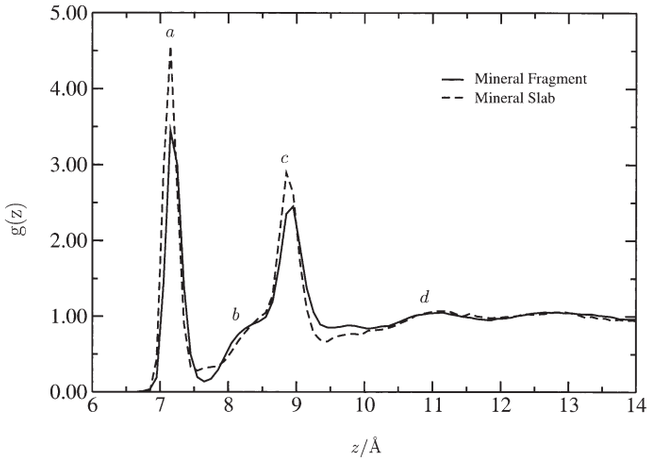

FIGURE 7 The radial distribution function for the mineral fragment. The *z*-axis represents the distance of water oxygen atoms to $z = 0$, which corresponds to the center of the mineral. The distribution is restricted to water atoms above the (110) mineral surface.

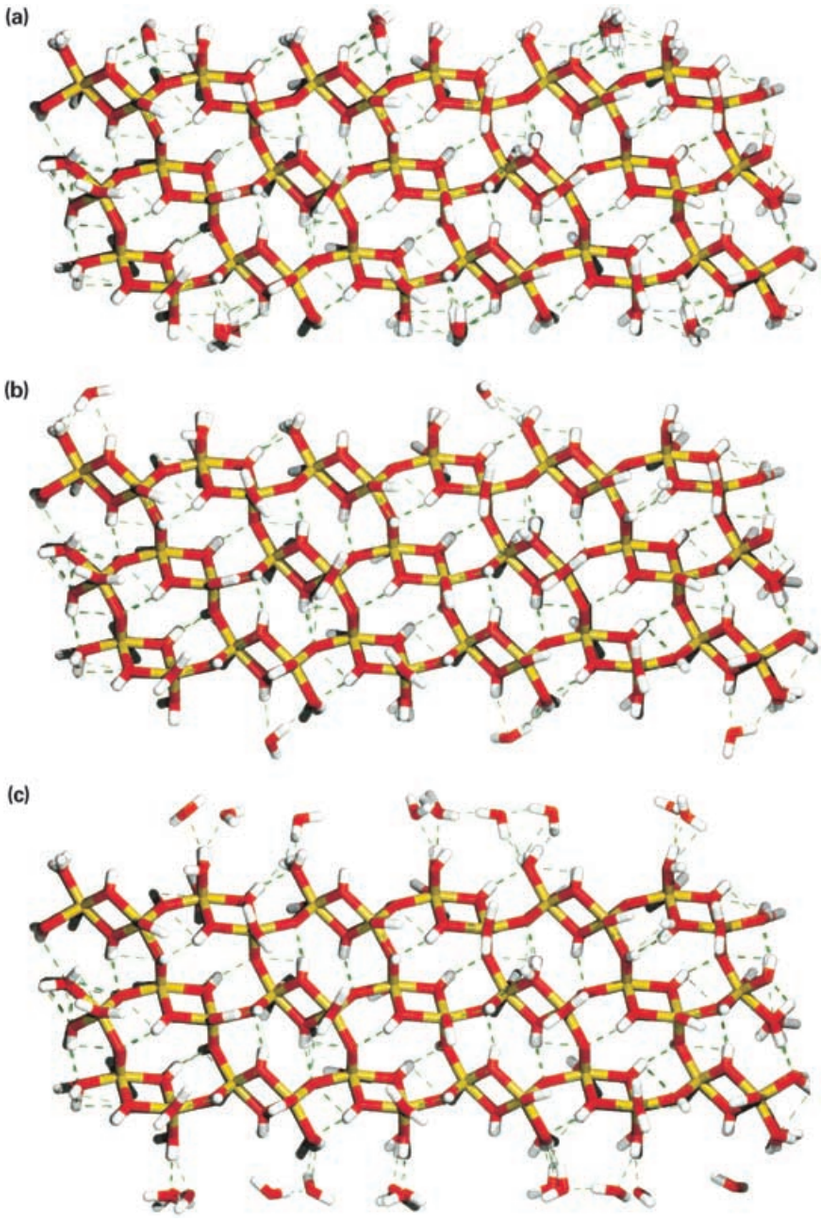

FIGURE 8 Snap shots of the mineral fragment in water. Iron atoms are rendered in gold, oxygen atoms in red, and hydrogen atoms in white. Water molecules are displayed for regions of the $g(z)$ plot shown in Fig. 7. Hydrogen bonds are represented by green dashed lines and were shown for non-bonded O–H distances that are less than the sum of the van der Waals radii. (a) A configuration displaying the water molecules of peak *a* from Fig. 7, where $z = 0.0$ Å to $z = 7.4$ Å. Water molecules in this region are close to the mineral surface. They are arranged in six rows parallel to the *x*-axis (Fig. 1a), which is normal to the plane of the page. (b) A configuration displaying the water molecules of peak *b* from Fig. 7, where $z = 8.0$ Å to $z = 8.4$ Å. Water molecules in this region typically form multiple hydrogen bonds to the mineral surface. (c) A configuration displaying the water molecules of peak *c* from Fig. 7, where $z = 8.7$ Å to $z = 9.1$ Å. Water molecules in this region typically form single hydrogen bonds to the mineral surface. (Colour version available online)

the sampling volume, which was determined by scaling the sum of the cylinder volumes by the ratio of uniquely sampled water molecules to the total number found in all cylinders. This method of sampling was used in order to view the water molecules next to the (110) surface of the fragment only (excluding the water structure of the fragment edges), facilitating comparison between the slab and fragment models. The center of the mineral corresponds to $z = 0$ on the graph and is oriented in the same manner as in Fig. 1b. Four peaks are evident near the surface of both mineral models and labeled *a*, *b*, *c*, and *d* in order of their increasing distances from the surface.

Three snap shots for the mineral fragment are displayed in Fig. 8a–c. These images show water molecules taken from *z*-axis regions corresponding to the first three peaks in Fig. 7. Configurations

represent water molecules sampled by the radial distribution function in the region of the peak. Only water molecules falling outside of the sampling area were excluded. A snap shot of peak *d* was excluded since the region is too distant for hydrogen bonding to the surface. All configurations were taken from the same time step, which was chosen at random.

Water molecules for peak *a* in Fig. 7 are shown in Fig. 8a. The peak is tall, thin, and the right side nearly touches the $g(z) = 0$ baseline. This is indicative of tightly bound water molecules and their exchange with bulk solvent is slow or non-existent. The configuration snap shot for this peak shows water molecules forming a row across the surface of the mineral. Molecules are oriented with one hydrogen pointed down toward a mineral surface oxygen atom forming a hydrogen bond. These surface oxygens are bound to three iron atoms and no hydrogens. Their point charges fall between -1.42 and -1.12 as shown in Fig. 4. Other hydrogen bonds are established between water molecules and neighboring surface hydroxyl groups (on either side of the water molecule row) or with water molecules to one another.

The second peak going out from the mineral surface is labeled *b* and a configuration snap shot for this peak is shown in Fig. 8b. Water molecules in this region still have the opportunity to form multiple hydrogen bonds with surface hydroxyl groups. Solvent molecules from peak *b* also form hydrogen bonds with those of peak *c*. They are located close to peak *c* and the formation of the second hydrogen bond pulls them slightly closer to the mineral surface. The water molecules of peak *c* form single hydrogen bonds to the mineral either through their oxygen or hydrogen atoms. The solvent molecules of peaks *b* and *c* form a water layer over the surface of the goethite mineral with an increased density compared to bulk water. Water molecules in this region would compete with ions or organic molecules for interaction sites on the goethite surface. The existence of this layer will therefore play an important role in adsorption processes at the goethite surface. Finally, the water molecules of peak *d*, for which a configuration snap shot is not shown, form a broad peak around 4 Å from the location of peak *a*. These molecules are too far from the mineral surface to directly hydrogen bond to it. They are most likely the result of hydrogen bonds between water molecules of peak *d* with those of peak *c*. There is no significant solution structuring beyond this distance. The experimental results of Cheng *et al.* [11] show similar water density oscillations for the mica–water system as those reported here.

The radial distribution functions show the average water molecule location relative to the mineral surface but do not contain information about the orientation of the molecules. Orientation structuring occurs near the surface of the mineral, further altering the properties of the water from those of bulk solution. The average orientation of the water molecule dipoles is shown in Fig. 9a–d. The water dipole points from negative to positive and is coincident with the molecular C_2 axis. The angle of the dipole with respect to the *z*-axis (shown in Fig. 1b) is θ, where $0 \leq \theta \leq 180$. For $\theta = 0°$ the dipole points away from the surface and for $\theta = 180°$ the dipole points toward the surface. The angle of the *xy*-projection of the dipole with respect to the *y*-axis is ϕ, where $0 \leq \phi < 360$. With respect to Fig. 1a, the dipole projection points down the page for $\phi = 0°$, to the left for $\phi = 90°$, up the page for $\phi = 180°$, and to the right for $\phi = 270°$. The probability that the water dipole has a given orientation of θ and ϕ is given by,

$$P(\theta, \phi) = P(\theta)P(\phi) \tag{1}$$

$$P(>) = \frac{\langle h(>)\rangle}{\langle n\rangle N(>)} \text{ and } \{ > |\theta, \phi\}, \tag{2}$$

where $P(\theta)$ and $P(\phi)$ are the probabilities that the dipole has an orientation with the specified angles, $\langle h(>)\rangle$ is the average number of dipoles of a given orientation, $\langle n\rangle$ is the average total number of dipoles sampled, and $N(>)$ is the angular dependent normalization. The angular dependence of N is only necessary for $P(\theta)$ because the sampling volume is a ring whose diameter is a function of the angle.

The orientation probabilities for water molecules in peak *a* of Fig. 7 are shown in Fig. 9a. Of all the radial distribution peaks, molecules in this region show the strongest deviation from bulk orientation. The figure shows two main peaks at ($\theta = 124°$, $\phi = 112°$) and ($\theta = 124°$, $\phi = 248°$) corresponding to rows of water molecules, which are evident in Fig. 8a. The water molecules are oriented with one hydrogen directed toward the mineral surface. The other hydrogen points in the direction of the next water molecule in the row. These may point in the positive or negative *x*-axis direction, thus forming two orientation peaks. The peaks are not located at values of ϕ that are exactly 180° from each other due to the water molecules rotating about the hydrogen atoms directed toward the surface and forming additional hydrogen bonds with mineral hydroxyl groups. The orientation $\theta = 124°$ is strongly favored, giving these solvent rows a net dipole moment with a *z*-projection pointing toward the mineral surface.

The orientation probabilities for water molecules in peak *b* of Fig. 7 are shown in Fig. 9b. There are three main probability peaks. A number of configurations were observed at various times during the simulation and all water molecules with dipoles within $\pm 5°$ of the peak values for θ and ϕ were found forming multiple hydrogen bonds to mineral surface hydroxyl groups. Peak *b* of Fig. 7 has a net dipole with a magnitude less than that of peak *a*.

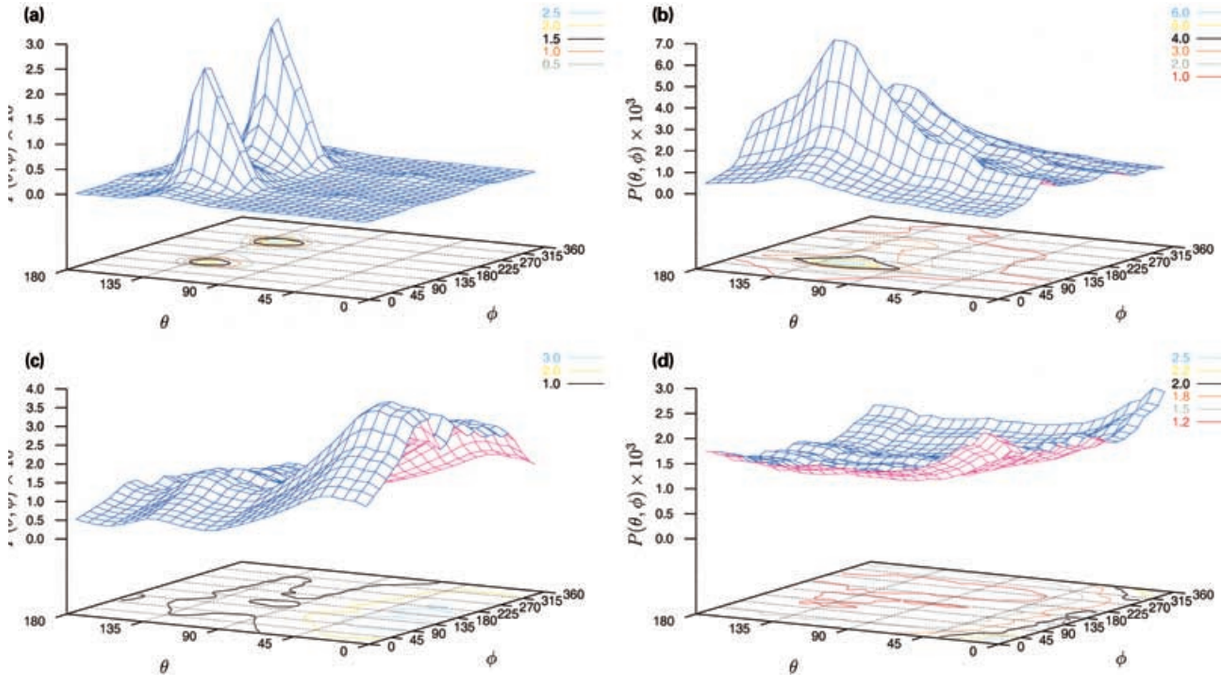

FIGURE 9 The probability P of finding the water molecule dipoles with an orientation determined by θ and ϕ. The angle of the dipole with an axis normal to the plane of the mineral surface is θ, where $0 \leq \theta \leq 180$. For $\theta = 0°$ the dipole points away from the surface and for $\theta = 180°$ the dipole points toward from the surface. The angle that determines the orientation of the vector in the plane of the surface is ϕ, where $0 \leq \phi < 360$. With respect to Fig. 1a, the dipole points down the page for $\phi = 0°$, to the left for $\phi = 90°$, up the page for $\phi = 180°$, and to the right for $\phi = 270°$. Orientation of the water molecule dipole of Fig. 7: (a) peak *a*; (b) peak *b*; (c) peak *c*; (d) peak *d*. (Colour version available online)

The orientation probability for water molecules in peaks *c* and *d* are shown in Fig. 9c,d. The orientation surface for the radial distribution peak *c* shows that the *z*-projection of the net dipole points away from the mineral surface. The *xy*-projection will be small in magnitude and point toward negative *y*. The orientation results for peak *d* show a situation approaching bulk water behavior.

CONCLUSIONS

The slab model for goethite is appropriate for simulations such as predicting the adsorption free energy for organic molecules. Here the rigid nature of the mineral does not place unwanted restraints on the adsorbate. However, care must be taken to insure that the periodic mineral images are far enough apart so the confined solvent has bulk properties. The fragment model alleviates the structural effects that result from confining solvent molecules into slit pores and allows water molecules to flow between its surface and another without the use of grand ensemble methods [36]. It is also small enough to avoid the long equilibration times associated with water adsorption from the edges of layered systems. Most importantly for our future use of the model in biogeochemical studies, rigid constraints associated with periodic cell lengths in the plane of slab models have been removed while retaining realistic model behavior.

The mineral fragment model developed here reproduces the behavior of the goethite (110) surface with minimum influence of the edges. This was done by parameterizing the mineral atom-centered point charges using the results of a 2D-periodic Hartree–Fock calculation of the bulk slab. The result is a fragment model that accurately reproduces the electrostatic signature of the goethite surface as calculated from *ab initio* methods. The slab and fragment models are in close agreement on the structural features of mineral–water interface. Therefore no significant measurable effects, due to the existence of the edges, were witnessed in the structural characteristics of the solvent molecules located above the fragment surface.

Simulations of the water–mineral interface show distinct structural characteristics of solvent molecules near the surface. Four solution regions are clearly evident from the radial distribution functions of Fig. 7. Each region has its own unique hydrogen-bonding network. The mineral's influence on water structure is clearly seen for about 5.5 Å from the first solvent accessible plane near the mineral surface out into solution. A small group of molecules interacts strongly with the surface and their exchange with bulk solution is limited. Further from the mineral

surface, the water molecules form a layer with increased density relative to that of bulk. Molecules of this layer form hydrogen bonds directly to the mineral surface and with each other. These average structural features of the solution possess anisotropic molecular orientations, which result in net dipole moments. This behavior is related to the mineral's hydration thermodynamics and will affect adsorption processes at its surface.

Acknowledgements

The authors thank Andrew R. Felmy and James R. Rustad for providing goethite mineral coordinate files and for helpful discussion as well as Kevin M. Rosso and Edoardo Apra for assistance with the solid state calculations. The Geosciences Research Program of the U.S. Department of Energy, Office of Basic Energy Sciences supported this work. Computing resources were available through a Computational Grand Challenge Application grant from the Molecular Science Computing Facility in the Environmental Molecular Sciences Laboratory, which is operated with funding from the Office of Biological and Environmental Research. The NWChem 4.0 computational chemistry package for massively parallel computers used in this study was developed by the High Performance Computational Chemistry group, Environmental Molecular Sciences Laboratory, Pacific Northwest National Laboratory. Battelle Memorial Institute operates Pacific Northwest National Laboratory for the U.S. Department of Energy.

References

[1] Schwertmann, U. and Cornell, R.M. (1991) *Iron Oxides in the Laboratory: Preparation and Characterization* (Wiley-VCH, New York).
[2] Hayes, K.F., Roe, A.L., Brown, G.E., Hodgson, K.O., Leckie, J.O. and Parks, G.A. (1987) "*In situ* X-ray absorption study of surface complexes: selenium oxyanions on α-FeOOH", *Science* **238**, 783.
[3] Rustad, J.R., Felmy, A.R. and Hay, B.P. (1996) "Molecular statics calculations of proton binding to goethite surfaces: a new approach to estimation of stability constants for multisite surface complexation models", *Geochim. Cosmochim. Acta* **60**, 1563.
[4] Weidler, P.G., Schwinn, T. and Gaub, H.E. (1996) "Vicinal faces on synthetic goethite observed by atomic force microscopy", *Clays Clay Miner.* **44**, 437.
[5] Cornell, W.D., Cieplak, P., Bayly, C.I., Gould, I.R., Merz, K.M., Ferguson, D.M., Spellmeyer, D.C., Fox, T., Caldwell, J.W. and Kollman, P.A. (1995) "A second generation force field for the simulation of proteins, nucleic acids and organic molecules", *J. Am. Chem. Soc.* **177**, 5179.
[6] Lins, R.D. and Straatsma, T.P. (2001) "Computer simulation of the rough lipopolysaccharide membrane of *Pseudomonas aeruginosa*", *Biophys. J.* **81**, 1037.
[7] Teppen, B.J., Rasmussen, K., Bertsch, P.M., Miller, D.M. and Schäfer, L. (1997) "Molecular dynamics modeling of clay minerals: 1. Gibbsite, kaolinite, pyrophyllite, and beidellite", *J. Phys. Chem.* **101**, 1579.
[8] Yu, C.H., Norman, M.A., Miller, D.M., Teppen, B.J. and Schäfer, L. (2000) "Molecular dynamics simulations of the absorption of proteins on clay mineral surfaces", *J. Mol. Struct.* **556**, 95.
[9] Fenter, P., Teng, H., Geissbühler, P., Hanchar, J.M., Nagy, K.L. and Sturchio, N.C. (2000) "Atomic-scale structure of the orthoclase (001)-water interface measured with high-resolution X-ray reflectivity", *Geochem. Cosmochem. Acta* **64**, 3663.
[10] Fenter, P., McBride, M.T., Srajer, G., Sturchio, N.C. and Bosbach, D. (2001) "Structure of barite (001)- and (210)-water interfaces", *J. Phys. Chem. B* **105**, 8112.
[11] Cheng, L., Fenter, P., Nagy, K.L., Schlegel, M.L. and Sturchio, N.C. (2001) "Molecular-scale density oscillations in water adjacent to a mica surface", *Phys. Rev. Lett.* **87**, 156101–156103.
[12] Hass, K.C., Schneider, W.F., Curioni, A. and Andreoni, W. (1998) "The chemistry of water on alumina surfaces: reaction dynamics from first principles", *Science* **282**, 265.
[13] Hiemstra, T., Venema, P. and van Riemsdijk, W.H. (1996) "Intrinsic proton affinity of reactive surface groups of metal (hydr)oxides: the bond valence principle", *J. Colloid Interface Sci.* **184**, 680.
[14] Kollman, P.A. (1996) "Advances and continuing challenges in achieving realistic and predictive simulations of the properties of organic and biological molecules", *Acc. Chem. Res.* **29**, 461.
[15] Duan, Y. and Kollman, P.A. (1998) "Pathways to a protein folding intermediate observed in a 1-microsecond simulation in aqueous solution", *Science* **282**, 740.
[16] Smith, P.E. and van Gunsteren, W.F. (1994) "Consistent dielectric properties of the simple point charge and extended simple point charge models at 277 and 300 K", *J. Chem. Phys.* **100**, 3169.
[17] van der Spoel, D., van Maaren, P.J. and Berendsen, H.J.C. (1998) "A systematic study of water models for molecular simulation: derivation of water models optimized for use with a reaction field", *J. Chem. Phys.* **108**, 10220.
[18] Smith, P.E. and van Gunsteren, W.F. (1995) "Reaction filed effects on the simulated properties of liquid water", *Mol. Sim.* **15**, 233.
[19] Svishchev, I.M. and Kusalik, P.G. (1994) "Dynamics in liquid H_2O, D_2O, and T_2O—a comparative simulation study", *J. Phys. Chem.* **98**, 728.
[20] Giammonar, D.A. (1984) *An Examination of Conformational Flexibility in Porphyrins and Bulky-ligand Binding in Myoglobin* Ph.D ThesisUniversity of California (Davis, CA).
[21] Rustad, J.R., Felmy, A.R. and Hay, B.P. (1996) "Molecular statics calculations for iron oxide and oxyhydroxide minerals: toward a flexible model of the reactive mineral–water interface", *Geochim. Cosmochim. Acta* **60**, 1553.
[22] Ryckaert, J.P., Ciccotti, G. and Berendsen, H.J.C. (1977) "Numerical integration of the cartesian equations of motion of a system with constraints: molecular dynamics of *N*-alkanes", *J. Comp. Phys.* **23**, 327.
[23] Bayly, I.C., Cieplak, P., Cornell, W.D. and Kollman, P.A. (1993) "A well-behaved electrostatic potential based method using charge restraints for deriving atomic charges: the RESP model", *J. Phys. Chem.* **97**, 10269.
[24] Harrison, R.J., Nichols, J.A., Straatsma, T.P., Dupuis, M., Bylaska, E.J., Fann, G.I., Windus, T.L., Apra, E., Anchell, J., Bernholdt, D., Borowski, P., Clark, T., Clerc, D., Dachsel, H., de Jong, B., Deegan, M., Dyall, K., Elwood, D., Fruchtl, H., Glendenning, E., Gutowski, M., Hess, A., Jaffe, J., Johnson, B., Ju, J., Kendall, R., Kobayashi, R., Kutteh, R., Lin, Z., Littlefield, R., Long, X., Meng, B., Nieplocha, J., Niu, S., Rosing, M., Sandrone, G., Stave, M., Taylor, H., Thomas, G., van Lenthe, J., Wolinski, K., Wong, A. and Zhang, Z. NWChem, A Computational Chemistry Package for Parallel Computers, Version 4.0.1. Pacific Northwest National Laboratory, Richland, Washington 99352-0999, USA, 2001.
[25] Dovesi, R., Saunders, V.R., Roetti, C., Harrison, N.M., Causá, M., Orlando, R. and Zicovich-Wilson, C.M. (1998) *CRYSTAL98 User's Manual* (University of Torino, Torino).
[26] Saunders, V.R., Freyria-Fava, C., Dovesi, R., Salasco, L. and Roetti, C. (1992) "On the electrostatic potential in crystalline systems where the charge density is expanded in Gaussian functions", *Mol. Phys.* **77**, 629.
[27] Dovesi, R., Orlando, R., Roetti, C., Pisani, C. and Saunders, V.R. (2000) "The periodic Hartree–Fock method and its

implementation in the CRYSTAL code", *Phys. Stat. Sol.* **217**, 63.
[28] Rassolov, V., Pople, J.A., Ratner, M. and Windus, T.L. (1998) "6-31G* basis set for atoms K through Zn", *J. Chem. Phys.* **109**, 1223.
[29] Francl, M.M., Petro, W.J., Hehre, W.J., Binkley, J.S., Gordon, M.S., DeFrees, D.J. and Pople, J.A. (1982) "Self-consistent molecular-orbital methods. XXIII. A polarization-type basis set for 2nd-row elements", *J. Chem. Phys.* **77**, 3654.
[30] Hariharan, P.C. and Pople, J.A. (1973) "The influence of polarization functions on molecular orbital hydrogenation energies", *Theor. Chim. Acta* **28**, 213.
[31] Becker, U., Hochella, M.F. and Apra, E. (1996) "The electronic structure of hematite{001} surfaces: applications to the interpretation of STM images and heterogeneous surface reactions", *Am. Mineralogist* **81**, 1301–1314.
[32] Berendsen, H.J.C., Postma, J.P.M., van Gunsteren, W.F., DiNola, A. and Haak, J.R. (1984) "Molecular-dynamics with coupling to an external bath", *J. Chem. Phys.* **81**, 3684.
[33] Hockney, R.W. (1970) "The potential calculations and some applications", *Methods Comput. Phys.* **9**, 136.
[34] Essmann, U., Perera, L., Berkowitz, M.L., Darden, T., Lee, H. and Pedersen, L.G. (1995) "A smooth particle mesh ewald method", *J. Chem. Phys.* **103**, 8577.
[35] Berendsen, H.J.C., Grigera, J.R. and Straatsma, T.P. (1987) "The missing term in effective pair potentials", *J. Phys. Chem.* **91**, 6269.
[36] Shroll, R.M. and Smith, D.E. (1999) "Molecular dynamics simulations in the grand canonical ensemble: application to clay mineral swelling", *J. Chem. Phys.* **111**, 9025.

APPENDIX A

The goethite mineral model was developed within the AMBER force field. The potential energy of the mineral is therefore,

$$E_{\text{total}} = \sum_{\text{bonds}} K_r(r - r_{\text{eq}})^2 + \sum_{\text{angles}} K_\theta(\theta - \theta_{\text{eq}})^2 + \sum_{\text{dihedrals}} \frac{V_n}{2}[1 + \cos(n\phi - \gamma)] + \sum_{i<j} \left[\frac{A_{ij}}{R_{ij}^{12}} - \frac{B_{ij}}{R_{ij}^{6}} + \frac{q_i q_j}{\epsilon R_{ij}}\right], \quad \text{(A1)}$$

where K_r is the force constant for the bond length r, r_{eq} is the equilibrium bond length, K_θ is the force constant for the angle θ, θ_{eq} is the equilibrium bond length, V_n determines the magnitude of the dihedral potential, n is the number of minima in the dihedral potential term, ϕ is the dihedral angle, γ controls the dihedral potential phase, A_{ij} and B_{ij} are Lennard–Jones parameters, R_{ij} is the non-bonded distance between atoms, q_i is the charge on atom i, and ϵ is an R_{ij} dependent dielectric constant ($\epsilon = 1$ for this work). This is the same equation as used by Cornell *et al.* [5] and a detailed description may be found therein. The first two terms represent bonds and angles as a diagonal harmonic expression and third term is the dihedral potential. Intermolecular interactions are represented in the last term as a sum of a 6–12 potential and electrostatic interactions. Intramolecular electrostatic and van der Waals interactions are only calculated between atoms separated by at least three bonds.

Using the AMBER force field to parameterize the mineral model required the parameters r_{eq}, θ_{eq}, n, and γ from Eq. (A1). In order to reproduce the structure from Rustad *et al.* [3,21] new atom types were introduced, which differed from their AMBER counterparts only by the labels used (i.e. OH → Oa, Ob, etc.). This enabled us to reproduce the bonds, angles, and dihedrals of the mineral without introducing regions of internal stress. A computer program was developed for calculating equilibrium bonds, angles, and dihedrals for the goethite mineral model using AMBER style atom types. The program insured that duplicate atom types did not cause inconsistencies in the force field, which was further verified by analysis of intramolecular forces.